Journal of Colloid and Interface Science 708 (2026) 139704

Contents lists available at ScienceDirect

Journal of Colloid And Interface Science

journal homepage: www.elsevier.com/locate/jcis

Electrostatic interactions reshape the internal architecture of ionic microgels

Priti S. Mohanty [a,b,*], Chi Zhang [a], Elisa Ballin [c,d], Francesco Brasili [c,d], Giovanni Del Monte [e], Emanuela Zaccarelli [c,d,*], Frank Scheffold [a,*]

[a] Department of Physics, University of Fribourg, Chemin du Musée 3, 1700, Fribourg, Switzerland
[b] School of Chemical Engineering and School of Biotechnology, Kalinga Institute of Industrial Technology (KIIT) Deemed to be University, 751024, Bhubaneswar, Odisha, India
[c] Istituto dei Sistemi Complessi, Consiglio Nazionale delle Ricerche, Piazzale Aldo Moro 5, 00185, Roma, Italy
[d] Dipartimento di Fisica, Sapienza Università di Roma, Piazzale Aldo Moro 5, 00185, Roma, Italy
[e] Debye Institute for Nanomaterials Science, Utrecht University, Utrecht, Netherlands

ARTICLE INFO

Keywords:
Ionic microgels
Light scattering
Small-angle X-ray scattering
Numerical simulations
Electrostatics
Polymer networks

ABSTRACT

Incorporating ionic co-monomers into polymer microgels can alter their swelling behavior and introduce pH-responsiveness; however, their effect on the internal microgel structure remains poorly understood. Here we present a comprehensive study of poly(N-isopropylacrylamide-co-acrylic acid) microgels, revealing that the incorporation of ionic groups significantly alters their internal architecture. Using dynamic and static light scattering combined with small-angle X-ray scattering, we observe pronounced differences in form factors and swelling behavior between neutral and ionic microgels. These findings can be rationalized by monomer-resolved simulations, which reproduce the experimental form factors only when charge-induced alterations to the network architecture are explicitly accounted for during in silico synthesis. Our results demonstrate that electrostatic interactions modulate not only the swelling behavior but also the internal monomer density profile, highlighting the need to integrate and extend current modeling approaches for charged microgels.

1. Introduction

Microgels are soft colloidal particles composed of crosslinked polymer networks that can be made responsive to various stimuli, such as temperature, pH, ionic strength, and electric fields [37,39]. These particles can swell or shrink in solvents, and their tunable properties make them valuable model systems to study condensed matter physics problems [31,35,36] as well as excellent candidates for various applications, including drug delivery [22], tissue engineering [26], catalysis [20], and sensing [37]. Most research has focused on homopolymer microgels, such as the widely studied poly(N-isopropylacrylamide) (pNIPAM) and their temperature-dependent swelling behavior. In the case of the most widely used synthesis techniques, these microgels inherently embed ionic molecules stemming from the initiators that trigger the polymerization reaction; however, their concentration is typically low, and the resulting charges are concentrated at the surface. As a result, charge effects on the swelling behavior are often considered negligible, and microgels are generally treated as neutral [23,30], although this assumption has been questioned, particularly at low ionic strength [14,25].

In recent years, ionic microgels containing weak acidic or alkaline monomers have gained significant attention [10,33,34,49,50,53]. They are typically synthesized via a one-pot precipitation polymerization process, in which ionic comonomers such as acrylic acid (AA) are incorporated into the polymer network. The primary polymer is often pNIPAM, and the resulting co-polymer with acrylic acid is commonly referred to as p(NIPAM-co-AA) or simply as pNIPAM/pAA microgels [19,33]. These hybrid microgels can modulate their net charge in response to pH variations, due to the pH-dependent ionization of the acidic groups, which release H^+ ions upon dissociation. Consequently, ionic groups play a crucial role in influencing the swelling behavior and heterogeneity of microgel networks in response to changes in pH, temperature, and salt concentration [12,48].

Previous simulation studies [4] showed how the presence of charged monomers strongly influences the swelling and structural properties of polyelectrolyte nanogels, regulated by a strong interplay between degree of ionization, ionic strength and network topology. Other works focused on larger microgels [5–8,29], in which the extent of the external double layer is smaller than the particle size, differently from nanogels.

* Corresponding authors.
E-mail addresses: pritisundar.mohanty@kiitbiotech.ac.in (P.S. Mohanty), chi.zhang2@unifr.ch (C. Zhang), elisa.ballin@uniroma.it (E. Ballin), francesco.brasili@gmail.com (F. Brasili), giovanni.delmonte90@gmail.com (G. Del Monte), emanuela.zaccarelli@cnr.it (E. Zaccarelli), frank.scheffold@unifr.ch (F. Scheffold).

https://doi.org/10.1016/j.jcis.2025.139704
Received 3 September 2025; Received in revised form 10 December 2025; Accepted 15 December 2025
Available online 29 December 2025

These works analyzed the effect of ionization and salt concentration on the swelling and structural properties of microgel particles at high dilution, with different approaches based on a variety of assumptions on the inner conformation of the polymer network. Despite this amount of knowledge that allowed to understand the complex mechanisms that links ph and ionic strength with microgel swelling behavior, a comprehensive validation of these models with experiments directly looking into particles inner structure is still lacking for ionic microgels.

The swelling behavior of p(NIPAM-co-AA) microgels is strongly influenced by the deprotonation of AA groups [19,20]. In dilute conditions, it is governed by the pK_a, which is approximately 4.25 [33]. However, for polyelectrolytes (including microgels), electrostatic interactions usually increase the effective pK_a relative to that of AA monomer. As a result, substantial dissociation of −COOH groups occurs only at pH values well above the monomer pK_a. The presence of negatively charged groups ($-COO^-$) in the polymeric network leads to swelling of the microgel through two complementary mechanisms [1]. First, the negatively charged carboxylate groups on the polymer chains generate strong Coulombic repulsion, which drives chains apart and causes expansion of the network. Second, dissociated counterions, balancing the inner charge of the polymer network, induce an additional contribution to the osmotic pressure, known as the Donnan effect. Altogether, these electrostatic and osmotic contributions significantly enhance the swelling behavior of the microgel at a higher pH even above the lower critical solution temperature (LCST) of pNIPAM $T_{LCST} \simeq 33°C$. As a result, the volume phase transition (VPT) of the microgels occurs at a higher temperature T_{VPT}. Instead, when the pH is well below the monomer pK_a, the majority of carboxylic groups remain protonated (COOH). Under these conditions, ionic microgels show swelling behavior similar to that of the "neutral" ones, ie homopolymer microgels with charges provided only by the ionic initiator [21], with $T_{VPT} \simeq T_{LCST}$ [19,20,30].

The intricate interplay between electrostatic interactions and polymer network rearrangement adds complexity to microgel behavior, presenting a significant knowledge gap. Although the influence of ionic groups on the swelling behavior is known, it is often assumed that no significant alterations take place in the microgel's internal structure. In this scenario, the presence or absence of charges should only modulate electrostatic repulsion, which affects the rearrangement of the co-ion and counter-ion cloud, while the network itself should remain unchanged. However, this assumption has not yet been tested through a combined experimental and theoretical study, able to resolve in detail the microscopic structure of the microgels across the VPT.

Here, we demonstrate that pNIPAM microgels with a 5% crosslinker, synthesized both with and without an ionic comonomer, exhibit significant and unexpected differences in their internal structure. We systematically analyze the pH- and temperature-dependent form factors obtained through static light scattering (SLS) and small-angle X-ray scattering (SAXS). Notably, a comparison of the experimental form factors of the ionic microgels (at pH 7 and pH 3.5) with those of the neutral ones reveals that the presence of charged monomers strongly influences the internal network structure. This is further corroborated by the observation that the core–shell structure of the microgel at pH 3.5 differs significantly from that of the neutral microgel, contrary to expectations, given the near-complete charge neutralization at low pH in microgels containing AA groups. To shed light on the structural details of the microgel architecture at the molecular level, we compare experimental results with theoretical form factors derived from advanced in silico modeling under conditions that match the experiments [11,29]. This comparison demonstrates that the simulation protocol originally developed for neutral microgels is inadequate when ionic monomers are present. Our findings provide strong evidence that the internal network organization of neutral and ionic microgels is fundamentally different. We propose a tentative interpretation of these results in terms of altered (in-silico) synthesis conditions induced by the presence of ionic comonomers, laying the basis for experimental verification. Although beyond the scope of the present work, this needs to be verified in the future.

2. Materials and methods

2.1. Synthesis

Ionic p(NIPAM-co-AA) microgels were synthesized using precipitation polymerization, following the procedure reported in our earlier works [15,19,33]. In a typical polymerization process, NIPAM was used as monomer, N,N'-methylene-bis-acrylamide (BIS) as crosslinker, AA as ionic comonomer, and potassium persulfate (KPS) as initiator. The reaction mixture, containing the NIPAM, BIS and AA was purged with argon for 40 min and maintained under an argon atmosphere throughout the synthesis at a constant temperature of 70°C. Before starting the reaction, the pH of the reaction mixture was ∼3.5, lower than the pK_a of AA monomers. To maintain consistency with earlier works, we did not use any buffer to control pH during the reaction and still we are able to obtain reproducible microgels, as shown in Fig. S1[27]. Polymerization was initiated by adding KPS (0.036 g dissolved in 5 g of water). The polymerization process continued for 4 h and was ended by turning off the heat while maintaining the temperature at 70°C. The suspension was then allowed to cool under constant stirring overnight. Next, it was filtered through glass wool, and purified by repeated centrifugation, removal of the supernatant, and subsequent re-dispersion in Milli-Q water. The suspension was further dialyzed using Milli-Q water to ensure purity. Ionic microgels were prepared with 5 mol% BIS. For the preparation of neutral microgels, AA was omitted, while all other synthesis parameters remained unchanged. Table S1 in the Supplementary Material (SM)[27] summarizes the synthesis parameters.

2.2. Experimental characterization

Prior to characterization, all samples were thoroughly deionized using mixed bed ion-exchange resins to ensure a constant and low background ionic strength. This ensures ionic strength between 10^{-7}M and 10^{-6}M, corresponding to nearly zero-salt condition. SLS and dynamic light scattering (DLS) experiments were carried out using a 2D light scattering setup (LS Instruments, Switzerland) at a laser wavelength of 543 nm, to measure microgel form factors $P(q)$ and hydrodynamic radii (R_H), respectively. SLS data were obtained in the angular range between 20° and 140°. The reported form factors are the averages of five independent SLS measurements. For R_H measurements, the normalized correlation functions were analyzed using a second-order cumulant fit, where the estimated decay constant, $\Gamma = D_0 q^2$, provides the free diffusion constant D_0. From this, R_H was determined using the Stokes-Einstein equation, $D_0 = k_B T/(6\pi\eta R_H)$ [33], where k_B is the Boltzmann constant, T is the absolute temperature and η is the viscosity of the solvent water. R_H was measured at fixed scattering angles from 20° to 40° in steps of 5°, and the resulting values were averaged. The de-ionized samples exhibit a nominally neutral pH (∼ 7); no additional pH adjustment was carried out. Samples with pH 3.5 were prepared by adding HCL to the microgel suspension [19,33]. As shown in Fig. S2[27], a deswelling effect is observed in R_H for the 0.01 wt% sample at pH 7, while the results for 0.001 wt% and 0.003 wt% overlap, indicating that in this range the swelling is independent of microgel concentration. Consequently, all light scattering experiments shown in Fig. 1 were conducted at 0.001 wt%.

We analyzed the average intensity, together with the corresponding standard deviation at each q using the well established fuzzy-sphere model [32], which allowed us to determine the radius of the microgel core R_c and the shell fuzziness σ by fitting $P(q)$ to the function $|f(q)|^2$, with

$$f(q) = \frac{3\sin(qR_c) - 3qR_c\cos(qR_c)}{(qR_c)^3} \exp\left(-\frac{(q\sigma)^2}{2}\right) \quad (1)$$

which we also convolve with the suspension polydispersity (polydispersity index, PDI). This procedure gives a set of best-fit values for the core radius, shell thickness, and polydispersity. The parameters derived from

the SLS and DLS analyses, with the corresponding error bars, are summarized in Table S2[27].

SAXS experiments were performed at the ID02 beamline of the European Synchrotron Radiation Facility (ESRF). We measured highly diluted microgel dispersions (0.1 wt %) to exclude any contribution from interparticle correlations to the acquired patterns and thus to directly measure the microgel form factor $P(q)$, where the vector q is defined as $q = (4\pi/\lambda)\sin\theta$, 2θ is the scattering angle and λ is the wavelength of radiation. The samples were filled with capillaries (2 mm in diameter) and placed at the sample to detector distance of 31 m. Experiments were conducted at selected temperatures between 25 and 41° C using a Huber Ministat 230 thermostat. After each temperature change, the samples were left to thermalize for 10 min before measurements. The exposure time for the acquisitions was set to 0.5 s and, for each temperature, we acquired 10 scattering patterns using a two-dimensional Eiger2 X 4M detector (Dectris, Baden, Switzerland). This allows measurements in the range of q between 0.02 and 3.8 nm^{-1}. Scattering patterns of a capillary filled with water were recorded for background subtraction. The processing and averaging of the scattering patterns was performed with the SAXSutilities2 software [42]. When averaging, any scattering curve not perfectly superimposed on the acquired overall set, due to possible residual equilibration or other experimental perturbations, was discarded.

2.3. Numerical simulations

For numerical simulations, we use a coarse-grained model of the microgels, consisting of a disordered network of fully bonded $N = 112k$ spherical beads. Each of these monomers has diameter σ_m and mass m, which set the length and mass units, respectively. The *in silico* synthesis protocol assembling the microgels has been previously reported in Refs. [11] and [28]. The former reference describes a homogeneous assembly, while the second one introduces the presence of an effective force acting on the crosslinkers to give rise to the characteristic (heterogeneous) core-corona structure of pNIPAM-BIS microgels. Once the assembly is performed, the network is made permanent and interacting with the standard potential empolyed for polymers in good solvent. In particular, monomers interact via the bead-spring model established by Grest and Kremer [43], consisting of a steric repulsion for all beads and a bond term for connected ones. The bonds cannot break during the course of a simulation. The steric contribution is modeled by the Weeks–Chandler–Anderson (WCA) potential:

$$V_{\mathrm{WCA}}(r) = \begin{cases} 4\varepsilon\left[\left(\frac{\sigma_m}{r}\right)^{12} - \left(\frac{\sigma_m}{r}\right)^{6}\right] + \varepsilon & \text{if} \quad r \le 2^{1/6}\sigma_m \\ 0 & \text{if} \quad r > 2^{1/6}\sigma_m \end{cases} \tag{2}$$

where r is the center-to-center distance between a given pair of interacting beads and ε sets the energy scale. The bonded interaction is given by the Finitely Extensible Nonlinear Elastic (FENE) potential [29,44]:

$$V_{\mathrm{FENE}}(r) = -\epsilon k_F {R_F}^2 \ln\left[1 - \left(\frac{r}{R_F\sigma_m}\right)^2\right], \quad r < R_F\sigma_m \tag{3}$$

with $R_F = 1.5$ and $k_F = 15$. The FENE potential links monomers to two neighbors, representing segments of polymer chains, whereas crosslinkers are connected to four monomers. The fraction of crosslinkers is set to $c = 0.05$, as in experiments. To mimic charged monomers, we provide a varying fraction f of beads with a negative charge. In particular, we used $f = 0.075$ for pH 7 ionic microgels, similar to the nominal amount of added AA in experiments, and $f = 0.03$ for the same at pH 3.5. We also tested $f = 0.10$ and $f = 0.05$ and found no significant differences in the results. The experimental charges, that originate from covalently bound COOH groups, experience local fluctuations within the network, since the deprotonation/protonation state of AA is dynamically depending on pH. To simulate such dynamical charge fluctuations charge regulation mechanisms have been developed [5,9], consisting in Monte Carlo or hybrid algorithm that allow to simulate the protonation/deprotonation dynamics at fixed pH. Within the current simulation approach, we do not introduce such charge regulation mechanisms for a matter of convenience, since we use parallelized full Molecular Dynamics algorithm, given the need to simulate large sized systems, thus we assumed a fixed charge distribution in the course of the simulations and average over different distribution realizations. This is not qualitatively affecting our results, since we study the system only at pH that is small (large) with respect to the pK_a of AA, when acidic monomers are almost all (de-)protonated.

We simulate both homogeneous and heterogeneous microgels with different charge distributions, either by assigning charged beads randomly (random charge distribution), or by assigning them randomly only in the exterior corona of the microgel (surface charge distribution), i.e., where the distance from the center of mass of the microgel is greater than R_g. We also employed mixed random-surface distributions. Only the surface distribution was found to yield results in agreement with the experiments in all cases.

We also insert counterions, positively charged beads with diameter $\sigma_c = 0.1\,\sigma_m$, to ensure overall electroneutrality. Counterions interact with all other particles in the simulation through the WCA potential. Additionally, all charged particles interact with the Coulomb potential:

$$V_{\mathrm{coul}}(r) = z_i z_j \frac{\lambda_B}{r} k_B T\,, \tag{4}$$

where z_i and z_j are the valences of the interacting beads (-1 for the charged monomers of the microgel and $+1$ for counterions), $\lambda_B = e^2/(4\pi\epsilon_0\epsilon_r k_B T) = e^{*2}/(k_B T)$ is the Bjerrum length, $e^* = \sqrt{4\pi\epsilon_0\epsilon_r\sigma_m k_B T}$ the reduced charge unit, $k_B T$ the thermal energy, ϵ_0 and ϵ_r the vacuum and relative dielectric constants, and r is the distance expressed in units of σ_m respectively. At the experimental condition of our experiments, the value of e^* has the same order of magnitude of e, and fixing our reduced energy unit to $k_B T$ leads to $\lambda_B \sim \sigma_m$. The particle-particle-particle-mesh method [51] is adopted to appropriately account for the long-range nature of Coulomb interactions.

To model the change in solvent affinity of microgels induced by temperature, we use an additional effective solvophobic potential V_α, acting only on neutral monomers [52], implicitly accounting for monomer–solvent interactions [45]:

$$V_\alpha(r) = \begin{cases} -\varepsilon\,\alpha & \text{if} \quad r \le 2^{\frac{1}{6}}\sigma_m \\ \frac{1}{2}\,\alpha\,\varepsilon\left[cos(\gamma_0(r\sigma_m)^2 + \beta_0) - 1\right] & \text{if} \quad 2^{\frac{1}{6}}\sigma_m < r \le R_F\sigma_m \\ 0 & \text{if} \quad r > R_F\sigma_m \end{cases} \tag{5}$$

Here $\gamma_0 = \pi(2.25 - 2^{1/3})^{-1}$ and $\beta_0 = 2\pi - 2.25\gamma_0$. This is an attractive term, whose strength is modulated by the solvophobic parameter α, which can be considered as an effective temperature. Therefore, $\alpha = 0$ represents good solvent conditions, while the attraction between monomers increases as α increases, leading to microgel shrinkage. The general behavior echoes the worsening of the affinity of the polymer for the solvent when the temperature increases [11,46]. Following previous work [52,53], charged monomers on the microgel do not interact with the solvophobic potential, even when temperature increases, to ensure that their hydrophilic character is maintained throughout the investigated temperature range.

NVT simulations of single microgels are then performed with the LAMMPS simulation package [54] at the temperature fixed by $k_B T = \varepsilon$ in a cubic box with side $L = 400\,\sigma_m$ and periodic boundary conditions. The equations of motion are integrated with a time step $\Delta t = 0.002\,\tau$, where $\tau = \sqrt{m\sigma_m^2/\varepsilon}$ is the reduced time unit. We use the Nosé-Hoover thermostat in the constant NVT ensemble for equilibration ($1000\,\tau$) and the Velocity-Verlet algorithm in the constant-energy ensemble for the production runs ($20000\,\tau$). The latter are used to extract the equilibrium averages of the observables of interest.

The hydrodynamic radius R_H of microgels is computed from simulations using the method presented in ref. [53]. Briefly, we approximate

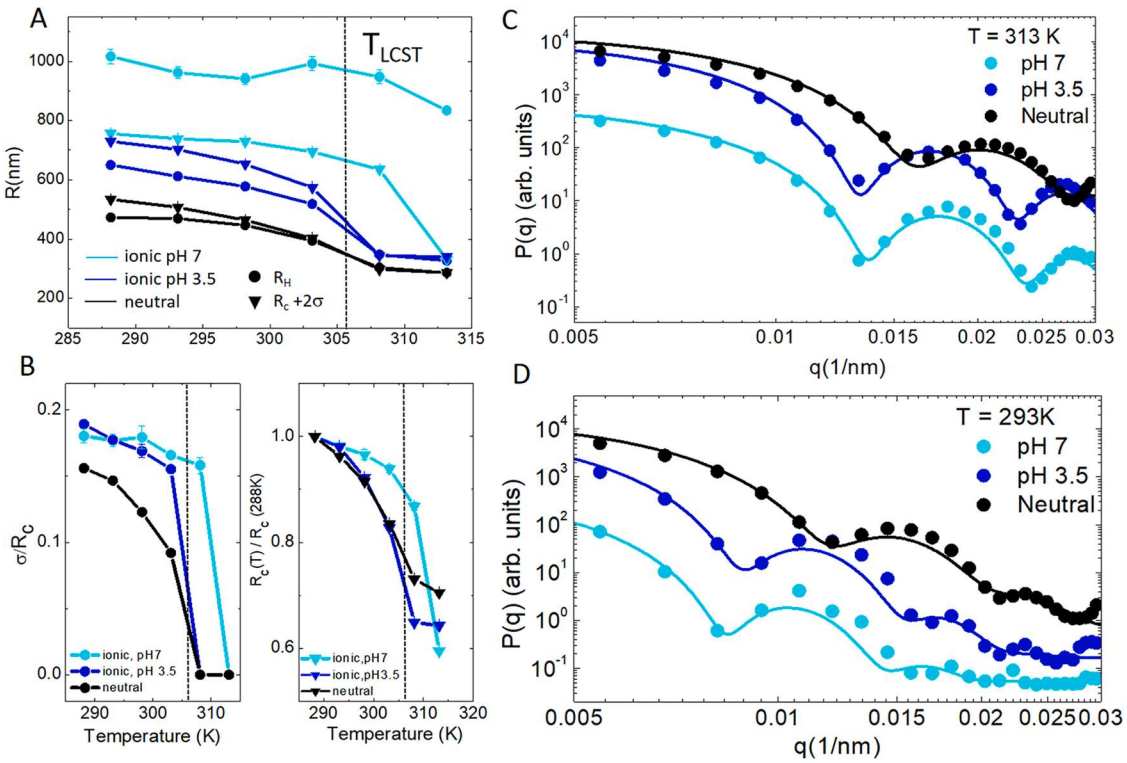

Fig. 1. (A) Swelling curves as a function of temperature, showing R_H measured by DLS as well as $R_c + 2\sigma$ obtained by fitting SLS form factors to the fuzzy-sphere model (Eq. (1)); R_c is the core radius and σ the fuzziness parameter. (B) comparison between the ratios σ/R_c and $R_c(T)/R_c(288K)$ (core swelling) as a function of temperature in first and second graph respectively. In A and B, the vertical dashed line represents T_{LCST} of pNIPAM homopolymer. Microgel form factors $P(q)$ as a function of q measured by SLS at $T = 313$ K (C) and $T = 293$ K (D). The form factors are averaged over five repeated measurements. In C and D, solid lines are the fits to the fuzzy sphere model.

the microgel as an ellipsoid with the same gyration tensor of the convex hull containing all the beads of the microgel. We then calculate R_H following the approach of Hubbard and Douglas [55]:

$$R_H = 2\left[\int_0^\infty \frac{1}{\sqrt{(a^2+\theta)(b^2+\theta)(c^2+\theta)}}\,d\theta\right]^{-1}, \quad (6)$$

where a, b and c are the principal semiaxes of the gyration tensor. The form factors of the microgels are calculated at each wavenumber q as

$$P(q) = \frac{1}{N}\sum_{i,j} e^{-i\vec{q}\cdot\vec{r}_{ij}}, \quad (7)$$

where $\vec{r}_{ij}$ is the distance between the ith and jth monomer.

3. Results and discussion

We start by characterizing the swelling behavior of the microgels using DLS and SLS at a very dilute concentration of 0.001 wt%, selected based on tests across a range of concentrations between 0.001 and 0.01 wt% (Fig. S2[27]). DLS allows us to measure the hydrodynamic radius R_H, which represents the global size that governs particle diffusion due to thermal motion, while SLS, along with SAXS, is sensitive to the polymer density gradient inside the particle, providing insights into the internal structure.

All experiments were performed according to standard procedures. By analyzing the pH conditions of deprotonated (pH = 7) and protonated (pH = 3.5) AA monomers and by tuning temperature over a wide range, we investigate how the internal structure of the microgel depends on its charge and solvent quality, which deteriorates above T_{LCST}. Fig. 1 reports DLS and SLS measurements for pNIPAM-co-pAA microgels at two different pH values, as well as for pure pNIPAM (neutral) microgels [21]. In Fig. 1A we present data of R_H as a function of temperature. The form factors $P(q)$, obtained by the angular resolved SLS data, are shown in Fig. 1C and D, for two different temperatures, as a function of the scattering wave vector q given by $q = 2k \sin\frac{\theta}{2}$, with the scattering angle denoted by θ and $k = \frac{2\pi n_h}{\lambda}$ being the wavenumber for the laser wavelength λ in water, where $n_h = 1.33$. They also exhibit significant differences in their overall form factors as shown in Fig. 1C and D. As expected, ionic microgels at pH 7 show swelling behavior different from the typical one of neutral microgels, due to the influence of charges and counterions. In particular, the experiments also reveal marked differences between ionic and "neutral" microgels, even when the pH is reduced to 3.5, neutralizing AA charges. Specifically, ionic microgels remain more swollen at all temperatures, showing a larger R_H, and, more surprisingly, they also exhibit significant differences in overall form factors, particularly at temperatures below T_{VPT}.

To gain more insight into the modifications of the internal core-shell structure of the microgels, we analyzed SLS data employing the fuzzy-sphere model reported in Eq. (1) [32], allowing us to determine the radius of the core R_c and the shell fuzziness σ. We find that this model fits the experimental data rather well at all temperatures and pH, despite the limited q-range probed. From these fits, also shown in Fig. 1C and D, we can extract information about the separate swelling of the core and shell regions, which cannot be obtained using DLS alone. Table S2[27] summarizes the parameters obtained from the fits.

We begin by analyzing the total size of the microgels, given by $R_c + 2\sigma$ (Fig. 1A). We find that $R_c + 2\sigma$ is significantly smaller than R_H for ionic microgels at pH 7. Examining the internal structure in more detail, we observe that the ratio σ/R_c is higher for ionic microgels as compared to neutral ones, particularly at pH 7 close to T_{LCST} (Fig. 1B), due to the strong electrostatic repulsion from fully deprotonated COO^- groups which results in a more extended corona. In addition, counterion

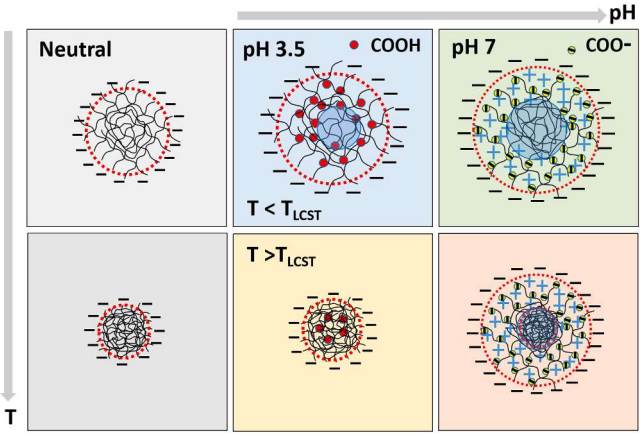

Fig. 2. Sketch of the microgels internal structure in their swollen and collapsed states, comparing neutral microgels with ionic AA-functionalized ones in their protonated (pH 3.5) and deprotonated (pH 7) states. Top row: $T < T_{VPT}$, swollen state; bottom row: $T > T_{VPT}$, collapsed state. Black minus signs represent initiator-derived charges, red circles are protonated COOH groups, yellow circles with a minus sign are deprotonated COO^- groups, and blue plus signs are the corresponding dissociated counterions. The red dotted line is a guide to the eye, indicating the microgel R_H. The sketch highlights the difference between the charge-free core and the charge-rich shell, which influence the swelling behavior of ionic microgels. While neutral microgels undergo a rather homogeneous deswelling, ionic microgels at low pH show a final collapsed structure that is different from neutral ones due to the presence of ionizable groups, affecting the internal network structure during synthesis. At high pH, ionic microgels display a much reduced tendency to collapse, due to the presence of a large amount of counterions in the periphery of the core, yielding the characteristic two-step density profile reported in Fig. 4. (For interpretation of the references to colour in this figure legend, the reader is referred to the web version of this article).

depletion in the periphery can lead to a localized osmotic imbalance, which may contribute to an enhanced swelling of the outer shell. This is also valid at low pH, where the degree of ionization is significantly reduced, but the σ/R_c ratio is still larger than that of neutral microgels. This is in agreement with the fact that the internal structure of the microgels at pH 3.5 does not exactly resemble that of neutral ones, as also evident in the form factors reported in Figs. 1C,D. Moreover, a small fraction of residual ionized groups and of their associated counterions can still influence the shell extension.

In addition, at pH 7, the swelling ratio of the core -defined as $R_c(T)/R_c(288\ \mathrm{K})$ and shown in Fig. 1B—remains nearly constant across T_{LCST}, exhibiting a sharp drop at the highest temperature investigated. At this T, the neutral microgels retain a higher swelling ratio than the ionic ones. In fact, for an initially expanded network (as seen at pH 7 and low temperatures), the reduction in relative size is more pronounced. Interestingly, this observation is reminiscent of the sharp collapse–deswelling transition at intermediate pH (in our case, pH – $pK_a \simeq 2.75$) recently described by Yuan and Curk [12]. The sharpness of the collapse/expansion dynamics is a key parameter for pH-driven, pH-responsive nanogel actuators. In summary, the SLS and DLS results demonstrate that the volume phase transition (VPT) of ionic microgels is shifted to higher temperatures, exceeding 40°C at pH 7.

We now propose a comprehensive interpretation of this complex experimental phenomenology, using the illustration in Fig. 2 as a guide. Based on the model of Hoare and McLean [13], we assume that AA monomers, which carry most of the charges, are predominantly located in the loosely crosslinked corona surrounding the microgel core at low temperatures. This assumption is also supported by the lower reactivity of AA compared to BIS crosslinker and NIPAM monomers [56], and by the tendency of AA monomers to maximize their mutual distance due to electrostatic repulsion upon deprotonation at higher pH.

In this picture, at low temperatures (first row in Fig. 2), the corona is more extended due to two effects: (i) the polymer network is intrinsically less compact in regions rich in AA monomers, since their presence reduces the hydrophobicity during synthesis, leading to less dense particle growth; and (ii) electrostatic repulsion between AA monomers further stretches the network. This interpretation is consistent with the values of σ/R_c shown in Fig. 1B, which, at and below T_{LCST} are highest for pNIPAM-co-pAA microgels at pH 7 and lowest for neutral ones. The extended corona also influences the behavior of deswelling with increasing temperature. In ionic microgels at pH 7, the shell remains swollen up to approximately 35°C, due to the high σ/R_c ratio, thus increasing T_{VPT} relative to T_{LCST}. In contrast, neutral microgels exhibit substantial shell contraction already around 30°C, with $T_{VPT} \approx T_{LCST}$. Ionic microgels at low pH display intermediate behavior, but do not fully resemble the neutral case, owing to the persistent influence of AA monomers during the synthesis on the structure. Moreover, the stretching of the shell also impacts the core: the outward pull from the extended corona causes the core to be larger in ionic microgels than in neutral ones.

The unexpectedly altered structure of ionic microgels, even when carboxyl groups are protonated, raises questions about the origin of these different swelling curves and density profiles. To shed light on this, we performed numerical simulations in which the microgel is reproduced at a monomer-resolved level. In an earlier work [28], Ninarello et al. compared neutral microgels to numerical model predictions and demonstrated that the *in silico* data are able to successfully reproduce the core-corona structure of the microgels. This was obtained through the adoption of a network assembly process taking into account the ability of crosslinking molecules to react much faster than NIPAM, thus obtaining a non-homogeneous internal structure of microgels [28]. This protocol was validated against several experimental systems [16,17,24] and was also extended to describe ionic microgels [29,34,53], but a comparison of the internal structure with the experimental data is still lacking. Because of the complex chemistry involved during synthesis, little is known about the influence of Coulomb interactions during network formation. As a result, previous numerical studies have typically neglected the presence of charges during the formation of the network, introducing them only afterwards, once the network has been generated. This severely constrains the model, but vastly simplifies the procedure and allows testing different charge arrangements in order to validate the model against experimental data [53]. Here we face an entirely different kind of situation. In ionic microgels, charges are intentionally copolymerized and designed into the network. As a consequence, we find that introducing charges post-assembly in the simulations - mimicking the ionic AA groups in networks originally developed to describe neutral microgels (i.e., with a heterogeneous distribution of crosslinkers following the fuzzy-sphere scenario - fails to accurately reproduce the experimental data, regardless of the arrangement (see Fig. S3[27]).

This is a novel and significant finding: the charges themselves influence the formation of the network within the synthesis and ultimately determine the final architecture of the microgel, as illustrated in the snapshots in Fig. 3. The top row shows a microgel assembled with a heterogeneous internal structure and decorated with negative charges arising from acrylic acid groups and initiators (A) under good solvent conditions ($\alpha = 0.0$). The corresponding slice in (B) shows that these charges are predominantly located on the outer surface of the microgel. Upon heating above the VPT, for $\alpha = 0.85$ the microgel adopts the distinctive structure shown in (C), characterized by a compact core surrounded by an unusually large corona that remains swollen at all temperatures. This very extended corona is too extreme and the simulated microgels display form factors that do not agree with the data (see Fig. S4[27]).

To remediate this situation, we assume that the presence of ionic groups alters the polymerization process itself. Specifically, the electrostatic interactions between these groups probably contribute to maintaining a more homogeneous distribution of crosslinkers throughout the microgel particles, preventing their typical accumulation toward the center observed in neutral microgels. To test this hypothesis, we first

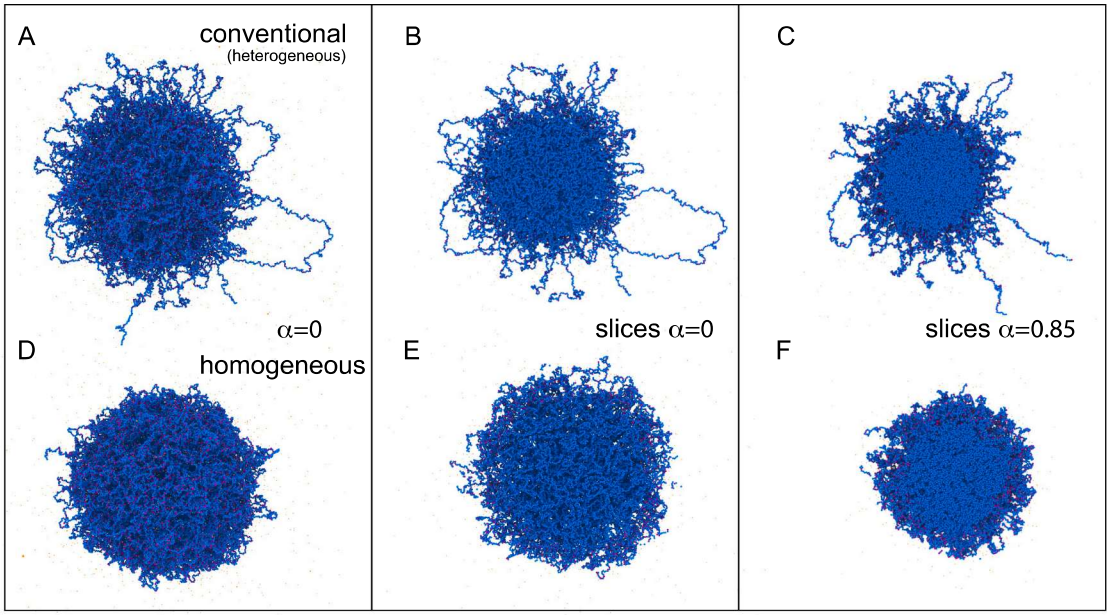

Fig. 3. Simulation snapshots from simulation, drawn to scale, illustrating the different assembly methods used for ionic microgels with crosslinker concentrations $c = 5\%$. Top row (A–C): conventional assembly of heterogeneous microgels, formed in the presence of a force acting on the crosslinkers, as described previously in Ref. [28]. Surface charges ($f = 0.075$) are added to mimic experimental conditions at pH 7. The simulated microgel are shown at low temperature ($\alpha = 0.0$) in full (A) and as a slice (B) to improve visualization of the charge-free inner part, as well as at high temperature ($\alpha = 0.85$, C). Bottom row (D–F): homogeneous microgels are assembled without the force acting on the crosslinkers and charges are again placed only on the surface. (D) low temperature ($\alpha = 0.0$) in full and as a slice (E) as well as at high temperature ($\alpha = 0.85$, F). In all panels, neutral (NIPAM) monomers are represented in blue, while ionic (AA or initiator) groups in purple. The small counterions are shown in orange. (For interpretation of the references to colour in this figure legend, the reader is referred to the web version of this article).

assembled homogeneous microgels and subsequently introduced the charges into the periphery. The bottom row of Fig. 3 shows a microgel with the same charge content as the top row, but now homogeneously assembled (D–F). The charges are again placed only on the surface, as illustrated in the (E) slice. This microgel exhibits a much more spherical shape than the previous one and, at high temperatures, collapses into a more compact structure decorated with a few dangling external chains bearing the charges (F). This modeling approach yields significantly improved agreement with the SLS experimental data. In fact, using the nominal molar concentration of crosslinkers and the known amount of AA, we are able to reproduce the experimental form factors at pH 7 with near-quantitative accuracy, as shown in Fig. 4A. Unfortunately, due to the complexity of ionic microgels, our coarse-grained modeling does not account for pH-dependent charge regulation, as achieved in Monte Carlo simulations at constant pH [18]. As a result, we have to manually reduce the number of charges in the model to reproduce the experimental observations at the lower pH.

In Fig. 4A, we therefore show a comparison between the model predictions and the SLS and SAXS experiments conducted at different temperatures and at two different pH values - above and below the pK_a of the ionic microgels. The SAXS and SLS data were found to agree quantitatively over the q range jointly covered by both techniques. The figure also includes the form factors of the neutral microgels synthesized under the same conditions, albeit without the addition of the charged comonomer. Numerically, neutral microgels are modeled using the standard protocol put forward in Ref. [28], that results in a heterogeneous network. The effective temperatures α used in the model, which control the solvent quality of the polymer, are the same for ionic microgels as those used for the neutral ones, making the model internally consistent. By appropriate adjustment of the charge density, we find excellent agreement between the experimental data and the model predictions, validating the accuracy of our approach. In contrast, Fig. S5[27] shows the results obtained when charges are directly added to the standard, heterogeneous network, which fails to reproduce the experimental behavior. It is also interesting that, if we remove the charges altogether, we obtain a different structure for neutral (initiator-only) microgels from the experimental data, since the latter are described by a heterogeneous crosslinker distribution. Interestingly, there is no way in which we can reconcile the two numerical approaches: indeed, even if we put only initiator charges on the homogeneous network, we do not recover the structure of the heterogeneous network in the absence of charges. This finding is illustrated in the SI, Fig. S4[27], where the direct comparison of the form factors in the two cases is reported, showing a clearly different behavior. This implies that the presence of the ionic comonomer necessarily alters the arrangement of the network during the synthesis, as further illustrated in Fig. S5[27].

Fig. 4B shows the radial polymer density profiles obtained from numerical simulations of the model, with homogeneous network and peripheral charges, that better reproduces experimental form factors. The corresponding spatial distributions of counterions are also shown in the figure alongside the polymer profiles. At pH 7 and for temperatures below the LCST, the microgel exhibits a low overall polymer density with a nearly flat core region, followed by gradual decay. This profile reflects a diffuse core–shell interface and a loosely crosslinked shell, characteristic of ionic microgels in their swollen state at high pH. Above the LCST, the density of the polymer increases significantly, indicating a more compact hydrophobic core, whereas overall the profile develops a clear two-step decay: an initial sharp drop at the core–shell boundary, followed by a more gradual decline. This feature likely reflects a heterogeneous polymer distribution in the shell, possibly influenced by the extended counterion cloud around the corona, through the Donnan effect. At pH 3.5 and below the LCST, the density profile shows a steeper decay than at pH 7, indicating a more compact and homogeneous structure due to reduced electrostatic repulsion of protonated carboxyl groups. Above the LCST, the overall density of the polymer remains high, similar to the case at pH 7. However, the two-step decay becomes less pronounced but still present, followed by a sharper drop, suggesting that the shell is significantly diminished and the core becomes more uniformly dense. In con-

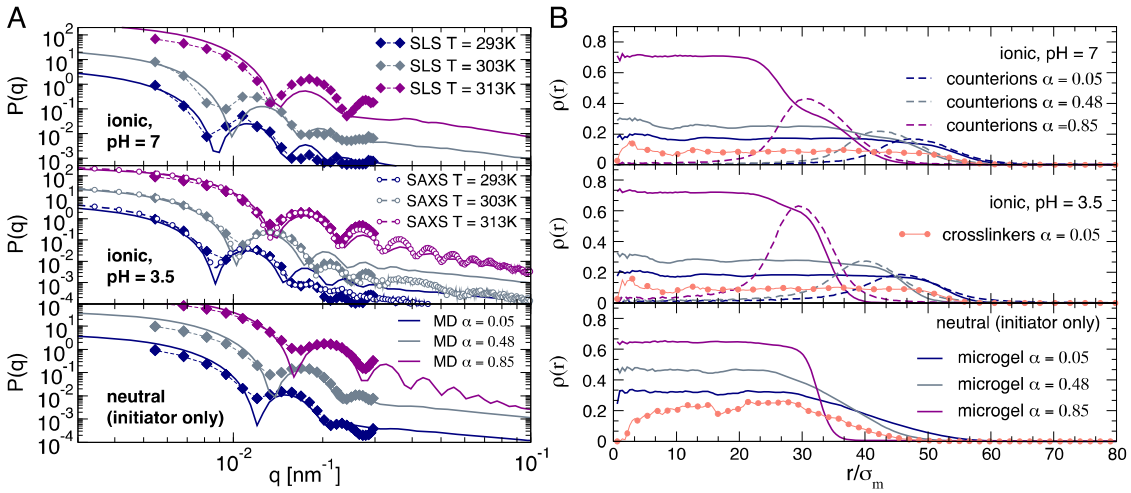

Fig. 4. Modeling of form factors for ionic microgels at pH 7 and pH 3.5, as well as for neutral microgels with $c = 5\%$. Comparison to scattering results. A) Scattering data are shown in the top to bottom graphs for $T = 293$, 303, and 313 K, respectively, and are compared in each case to numerical simulations at various α values. These values are consistent with those previously established for neutral microgels in Ref. [28]. The numerical model includes an internal force acting on the crosslinkers in the neutral case only, as explained in the text. B) Numerical density profiles of the microgel (full lines), of counterions only (dashed lines) and crosslinkers at lowest temperature (lines with symbols). Radial distances are expressed in units of the monomer diameter σ_m. The counterions profiles are multiplied by 10 and 30 for pH 7 and 3.5, respectively, while the crosslinkers profiles are multiplied by 10 in all cases, to improve readability of the figure.

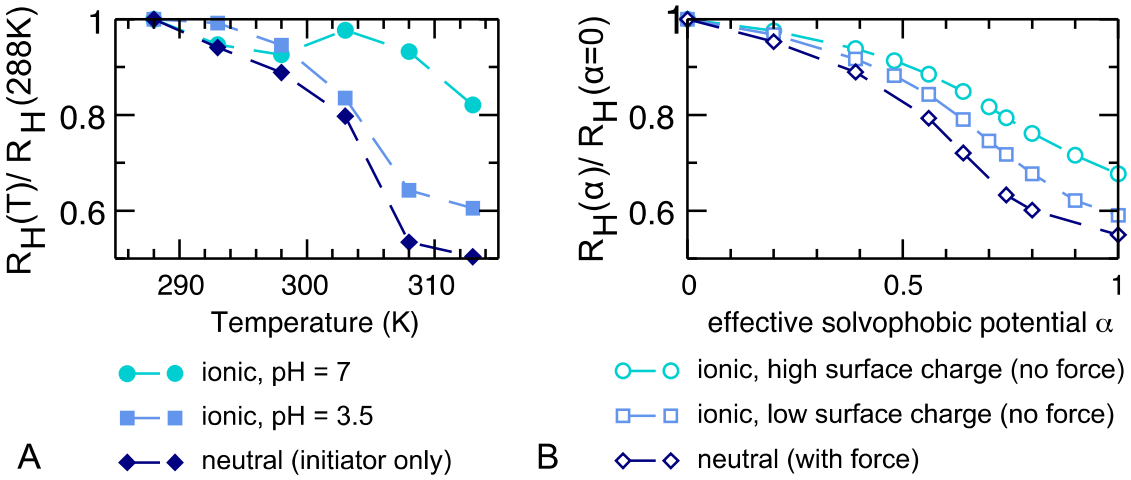

Fig. 5. Swelling ratio from experiments (A) and simulations (B).

trast, the neutral microgel displays a more extended decay in the low-temperature regime, reflecting a diffuse outer shell and a gradual decline in polymer density. At higher temperatures, the profile exhibits a single sharp drop, characteristic of a collapsed, dense core with negligible contribution from an outer shell. These findings clearly indicate that charge coupling between counterions and the polymer matrix plays a key role in shaping the internal microgel structure. In addition, we also report in Fig. 4B the crosslinker density profiles at the lowest temperature. In all cases, these follow rather closely the profiles of the whole microgel. This then directly visualizes the difference in the internal structure between neutral and ionic microgels, even at low pH, stemming from a different crosslinker distribution. This seems to be result of the fact that the fast polymerization kinetics of the crosslinker is somehow balanced by the accumulation of charged groups in the surface of the microgel, thus homogenizing the network in the ionic case with respect to the neutral one. Evidently, this difference cannot be resolved by lowering pH, being intrinsic of the different synthesis. Importantly these numerical results await further experimental validation, since the current SLS measurements are limited to a small wavevector range that is also compatible with the fuzzy sphere model, as shown in Fig. 1. While SAXS data are presently available only for the pH = 3.5 data, where the two-step decay is not completely evident, it would be important to measure these profiles directly, for example through super-resolution microscopy experiments, in order to visualize the internal arrangement of the charges and of the whole network [2,3,24].

In Fig. 5, we give an overview of the temperature dependence of the swelling ratio, derived from experimental and numerical swelling curves of R_H. The comparison demonstrates that the simulation approach employed also qualitatively captures these trends for all three types of microgels. Quantitative discrepancies with the experimental data remain due to the simplified model assumptions.

4. Conclusion

In conclusion, ionic microgels exhibit enhanced swelling under all conditions as compared to their neutral counterparts. The most pronounced swelling is observed in deprotonated microgels at pH 7, and this behavior persists even under poor solvent conditions. Above the lower critical solution temperature (T_{LCST}), some dangling chains, carrying charged hydrophilic groups, still extend from the microgel body, which explains the observed increase in hydrodynamic radius. The corresponding radial density profiles reveal clear structural differences between neutral and ionic microgels. At pH 7 ionic microgels display a distinct two-step decay: a weakly swollen core and a highly swollen, ex-

tended charged corona. Simulations are found to qualitatively support this structural scenario, providing interesting insights on the modifications taking place during the synthesis process due to the presence of a large amount of charged groups. Specifically, this leads to the need of a revision of the existing monomer-resolved modelling, the so-called *in silico* synthesis [11,28], when microgels are highly charged. Indeed, while for neutral microgels, the few initiator molecules are located preferentially on the surface, the simulation protocol needed to capture a microgel network with the characteristic core-corona structure includes the use of a phenomenological force on the crosslinkers [16,28]. Instead, when a signifcant amount of charged groups is included in the synthesis, we do not need to add this force, since otherwise the microgels become too heterogeneous, pushed by the long charged external chains. To mimic the correct experimental situation, it is thus sufficient to prepare a homogeneous network which is then stretched by the addition of the charges *a posteriori*. Hence, we speculate that the presence of many charged groups on the surface of the microgels competes with the tendency of the crosslinkers to accumulate in the core region, giving rise to an overall more homogeneous distribution of the crosslinkers throughout the microgels that cannot be recovered even lowering pH for ionic microgels with respect to neutral ones. Such different spatial distribution of the crosslinker with respect to the neutral microgels arises indirectly from the difference in polymerization rate between AA and NIPAm, as reported by Hoare and Pelton [57].

The robustness of these results is evidenced by the lack of agreement of the form factors evolution with temperature for microgels prepared without acrylic acid (neutral) and in the presence of 7.5% acrylic acid at low pH (visible in Fig. 1 for experiments and in Fig. S3[27] for simulations). In the future, these findings will need to be further extended by systematically varying the nominal amount of acrylic acid in order to determine the best protocol in the moderate presence of charges. In addition, similar experiments will need to be carried out for different amounts of crosslinkers within the synthesis, in order to validate and/or generalize the present results([27,38,40,41,47]). This will be the subject of future work.

CRediT authorship contribution statement

Priti S. Mohanty: Writing - original draft, Writing - review & editing, Visualization, Validation, Methodology, Investigation, Formal analysis, Data curation, Conceptualization; **Chi Zhang:** Writing - review & editing, Methodology, Investigation, Formal analysis, Data curation; **Elisa Ballin:** Writing - review & editing, Investigation; **Francesco Brasili:** Writing - review & editing, Investigation; **Giovanni Del Monte:** Writing - review & editing, Methodology, Investigation; **Emanuela Zaccarelli:** Writing - original draft, Writing - review & editing, Visualization, Supervision, Resources, Project administration, Methodology, Validation, Formal analysis, Data curation, Investigation, Funding acquisition, Conceptualization; **Frank Scheffold:** Writing - original draft, Visualization, Supervision, Resources, Project administration, Methodology, Investigation, Funding acquisition, Formal analysis, Conceptualization.

Data availability

Data will be made available on request.

Declaration of competing interest

The authors declare that they have no known competing financial interests or personal relationships that could have appeared to influence the work reported in this paper.

Acknowledgements

We thank ESRF for providing synchrotron radiation facilities and M. Sztucki for assistance during the measurements at the ID02 beamline and CINECA-ISCRA for HPC resources. This research was financially supported by the Swiss National Science Foundation (SNSF) through Grants No. 188494, 10002524. The project benefited from financial support by the Swiss National Centre of Competence in Research (NCCR) “Bio-Inspired Materials,” SNSF Grant No. 205603. EB and EZ acknowledge financial support by Progetto Co-MGELS funded by the European Union - NextGeneration EU under the National Recovery and Resilience Plan (PNRR) Mission 4 “Istruzione e Ricerca” - Component C2 - Investment 1.1 - “Fondo PRIN”, Project code PRIN2022PAYLXW Sector PE11, CUP B53D23008890006. EB, FB and EZ also acknowledge financial support from INAIL, project MicroMet (BRiC 2022, ID 16). PSM acknowledges KIIT Deemed to be University for granting duty leave to visit the University of Fribourg, Switzerland, to conduct research.

Supplementary material

Supplementary material associated with this article can be found in the online version at 10.1016/j.jcis.2025.139704.

References

[1] A. Fernández-Nieves, A. Fernández-Barbero, B. Vincent, F.J. de las Nieves, Charge controlled swelling of microgel particles, Macromolecules 33 (6) (2000) 2114–2118. https://doi.org/10.1021/ma991520l
[2] G.M. Conley, S. Nöjd, M. Braibanti, P. Schurtenberger, F. Scheffold, Superresolution microscopy of the volume phase transition of pNIPAM microgels, Colloids Surf. A 499 (2016) 18–23.
[3] S. Bergmann, O. Wrede, T. Huser, T. Hellweg, Super-resolution optical microscopy resolves network morphology of smart colloidal microgels, PCCP 20 (7) (2018) 5074–5083.
[4] L.G. Rizzi, Levin, Influence of network topology on the swelling of polyelectrolyte nanogels, J. Chem. Phys. 114 (11) (2016) 114903–114905. https://doi.org/10.1063/1.4943981
[5] C. Hofzumahaus, P. Hebbeker, S. Schneider, Monte Carlo simulations of weak polyelectrolyte microgels: pH-dependence of conformation and ionization, Soft Matter 14 (20) (2018) 4087–4100.
[6] H. Kobayashi, R. Halver, G. Sutmann, R.G. Winkler, Polymer conformations in ionic microgels in the presence of salt: theoretical and mesoscale simulation results, Polymers 9 (1) (2017) 15.
[7] A.R. Denton, Q. Tang, Counterion-induced swelling of ionic microgels, J. Chem. Phys. 145 (16) 011804 (2016).
[8] Y. Levin, A. Diehl, A. Fernández-Nieves, A. Fernández-Barbero, Thermodynamics of ionic microgels, Phys. Rev. E 65 (3) (2002) 036143.
[9] M.E. Brito, E. Höpner, D. Beyer, C. Holm, Modeling swelling of pH-responsive microgels: theory and simulations, Macromolecules 58 (5) (2025) 2494–2507.
[10] M.O. Alziyadi, A.R. Denton, Osmotic swelling behavior of surface-charged ionic microgels, J. Chem. Phys. 159 (18) (2023) 184901.
[11] N. Gnan, L. Rovigatti, M. Bergman, E. Zaccarelli, In silico synthesis of microgel particles, Macromolecules 50 (21) (2017) 8777–8786. https://doi.org/10.1021/acs.macromol.7b01600
[12] J. Yuan, T. Curk, Collapse/expansion dynamics and actuation of pH-responsive nanogels, arXiv preprint arXiv:2405.19193 (2024).
[13] T. Hoare, D. McLean, Kinetic prediction of functional group distributions in thermosensitive microgels, J. Phys. Chem. B 110 (41) (2006) 20327–20336. https://doi.org/10.1021/jp0643451
[14] B. Zhou, U. Gasser, A. Fernandez-Nieves, Measuring the counterion cloud of soft microgels using SANS with contrast variation, Nat. Commun. 14 (1) (2023) 3827.
[15] P.S. Mohanty, S. Nöjd, M.J. Bergman, G. Nägele, S. Arrese-Igor, A. Alegria, R. Roa, P. Schurtenberger, J. Dhont, Dielectric spectroscopy of ionic microgel suspensions, Soft Matter 12 (48) (2016) 9705–9727.
[16] N. Hazra, A. Ninarello, A. Scotti, J.E. Houston, P. Mota-Santiago, E. Zaccarelli, J.J. Crassous, Structure of responsive microgels down to ultralow cross-linkings, Macromolecules 57 (1) (2023) 339–355.
[17] E. Buratti, F. Camerin, V. Nigro, S. Franco, J. Ruiz-Franco, L. Porcar, R. Angelini, B. Ruzicka, Y. Gerelli, E. Zaccarelli, Fine-tuning the architecture of microgels by varying the initiator addition time, Soft Matter 21 (8) (2025) 1571–1582.
[18] C. Strauch, S. Schneider, Monte Carlo simulation of the ionization and uptake behavior of cationic oligomers into pH-responsive polyelectrolyte microgels of opposite charge–a model for oligopeptide uptake and release, Soft Matter 20 (6) (2024) 1263–1274.
[19] P.S. Mohanty, W. Richtering, Structural ordering and phase behavior of charged microgels, J. Phys. Chem. B 112 (2008). https://doi.org/10.1021/jp808203d
[20] P. Bhol, P.S. Mohanty, Smart microgel-metal hybrid particles of PNIPAM-co-PAA@AgAu: synthesis, characterizations and modulated catalytic activity, J. Phys. Condens. Matter 33 (2022). https://doi.org/10.1088/1361-648X/abbe79
[21] Note on the terminology of “neutral” microgels, 2025, So-called “neutral” microgels are not strictly neutral, since they are still synthesized in the presence of a small amount of ionic initiator (KPS). Conventionally, they are considered neutral in the following sense: weak residual charging, originating from the initiator, stabilizes the

suspensions against aggregation but is assumed to have no influence on the microgel internal structure.
[22] X. Shaulli, A.M. Moreno-Echeverri, M. Andoni, E. Waeber, S.N. Ramakrishna, C. Fritsch, D. Vanhecke, B. Rothen-Rutishauser, F. Scheffold, Polymer nano-carrier-mediated gene delivery: visualizing and quantifying DNA encapsulation using dSTORM, Small 21 (2025) 2405929.
[23] G.M. Conley, C. Zhang, P. Aebischer, J.L. Harden, F. Scheffold, Relationship between rheology and structure of interpenetrating, deforming and compressing microgels, Nat. Commun. 10 (1) (2019) 2436.
[24] X. Shaulli, R. Rivas-Barbosa, M.J. Bergman, C. Zhang, N. Gnan, F. Scheffold, E. Zaccarelli, Probing temperature responsivity of microgels and its interplay with a solid surface by super-resolution microscopy and numerical simulations, ACS Nano 17 (3) (2023) 2067–2078.
[25] S. Sennato, E. Chauveau, S. Casciardi, F. Bordi, D. Truzzolillo, The double-faced electrostatic behavior of PNIPAm microgels, Polymers 13 (7) (2021) 1153.
[26] Q. Feng, D. Li, Q. Li, X. Cao, H. Dong, Microgel assembly: fabrication, characteristics and application in tissue engineering and regenerative medicine, Bioact. Mater. 9 (2022) 105–119.
[27] Supplementary Materials for [Ionic groups unexpectedly modify the internal structure of microgels], 2025, Available as supplementary information.
[28] A. Ninarello, J.J. Crassous, D. Paloli, F. Camerin, N. Gnan, L. Rovigatti, P. Schurtenberger, E. Zaccarelli, Modeling microgels with a controlled structure across the volume phase transition, Macromolecules 52 (2019) 7584–7592.
[29] G. Del Monte, A. Ninarello, F. Camerin, L. Rovigatti, N. Gnan, E. Zaccarelli, Numerical insights on ionic microgels: structure and swelling behaviour, Soft Matter 15 (40) (2019) 8113–8128.
[30] F.A. Plamper, W. Richtering, Functional microgels and microgel systems, Acc. Chem. Res. 50 (2) (2017) 131–140.
[31] D. Paloli, P.S. Mohanty, J.J. Crassous, E. Zaccarelli, P. Schurtenberger, Fluid–solid transitions in soft-repulsive colloids, Soft Matter 9 (11) (2013) 3000–3004.
[32] M. Stieger, W. Richtering, J.S. Pedersen, P. Lindner, Small-angle neutron scattering study of structural changes in temperature sensitive microgel colloids, J. Chem. Phys. 120 (2004) 6197–6206.
[33] S. Nöjd, P. Holmqvist, N. Boon, M. Obiols-Rabasa, P.S. Mohanty, R. Schweins, P. Schurtenberger, Deswelling behaviour of ionic microgel particles from low to ultra-high densities, Soft Matter 14 (20) (2018) 4150–4159.
[34] R. Elancheliyan, G. Del Monte, E. Chauveau, S. Sennato, E. Zaccarelli, D. Truzzolillo, Role of charge content in the two-step deswelling of poly (N-isopropylacrylamide)-based microgels, Macromolecules 55 (17) (2022) 7526–7539.
[35] S. Ganguly, P.S. Mohanty, P. Schurtenberger, S. Sengupta, A. Yethiraj, Contrasting the dynamics of elastic and non-elastic deformations across an experimental colloidal martensitic transition, Soft Matter 13 (27) (2017) 4689–4697.
[36] M. Bergman, Y. Xu, J. Muñéton Díaz, C. Zhang, T.G. Mason, F. Scheffold, A free energy model for the plateau shear modulus in thermosensitive microgel suspensions, Langmuir 141 (6) (2025) 4084–4091.
[37] A. Fernandez-Nieves, H.M. Wyss, J. Mattsson, D.A. Weitz, Microgel Suspensions, Wiley, 2011.
[38] M.J. Bergman, S. Nöjd, P.S. Mohanty, N. Boon, J.N. Immink, J.J.E. Maris, J. Stenhammar, P. Schurtenberger, On the role of softness in ionic microgel interactions, Soft Matter 17 (2021). https://doi.org/10.1039/D1SM01222C
[39] T. Colla, P.S. Mohanty, S. Nöjd, E. Bialik, A. Riede, P. Schurtenberger, C.N. Likos, Self-assembly of ionic microgels driven by an alternating electric field: theory, simulations, and experiments, ACS Nano 12 (5) (2018) 4321–4337. https://doi.org/10.1021/acsnano.7b08843
[40] P.S. Mohanty, D. Paloli, J.J. Crassous, E. Zaccarelli, P. Schurtenberger, Effective interactions between soft-repulsive colloids: experiments, theory, and simulations, J. Chem. Phys. 140 (2014). https://doi.org/10.1063/1.4866644
[41] B.J. Berne, R. Pecora, Dynamic Light Scattering, John Wiley and Sons, New York,, 1976.
[42] M. Sztucki, SAXSutilities2: a graphical user interface for processing and analysis of small-angle X-ray scattering data, Zenodo (2021). https://doi.org/10.5281/zenodo.5825707
[43] G.S. Grest, K. Kremer, Molecular dynamics simulation for polymers in the presence of a heat bath, Phys. Rev. A 33 (5) (1986) 3628. https://doi.org/10.1103/PhysRevA.33.3628
[44] K. Kremer, G.S. Grest, Dynamics of entangled linear polymer melts: a molecular-dynamics simulation, J. Chem. Phys. 92 (8) (1990) 5057–5086. https://doi.org/10.1063/1.458541
[45] T. Soddemann, B. Dünweg, K. Kremer, A generic computer model for amphiphilic systems, Eur. Phys. J. E 6 (2001) 409–419. https://doi.org/10.1007/s10189-001-8054-4
[46] A.J. Moreno, F.L. Verso, Computational investigation of microgels: synthesis and effect of the microstructure on the deswelling behavior, Soft Matter 14 (34) (2018) 7083–7096. https://doi.org/10.1039/c8sm01407h
[47] M.J. Bergman, J.S. Pedersen, P. Schurtenberger, N. Boon, Controlling the morphology of microgels by ionic stimuli, Soft Matter 16 (11) (2020) 2786–2794.
[48] Y. Hertle, T. Hellweg, Thermoresponsive copolymer microgels, J. Mater. Chem. B 1 (43) (2013) 5874–5885.
[49] D. Capriles-González, B. Sierra-Martín, A. Fernández-Nieves, A. Fernández-Barbero, Coupled deswelling of multiresponse microgels, J. Phys. Chem. B 112 (39) (2008) 12195–12200.
[50] M. Karg, I. Pastoriza-Santos, B. Rodriguez-Gonzalez, R. Von Klitzing, S. Wellert, T. Hellweg, Temperature, pH, and ionic strength induced changes of the swelling behavior of PNIPAM- poly (allylacetic acid) copolymer microgels, Langmuir 24 (12) (2008) 6300–6306.
[51] M. Deserno, C. Holm, How to mesh up Ewald sums. I. A theoretical and numerical comparison of various particle mesh routines, J. Chem. Phys. 109 (18) (1998) 7678–7693. https://doi.org/10.1063/1.477414
[52] G. Del Monte, F. Camerin, A. Ninarello, N. Gnan, L. Rovigatti, E. Zaccarelli, Charge affinity and solvent effects in numerical simulations of ionic microgels, J. Phys. Condens. Matter 33 (8) (2020) 084001.
[53] G. Del Monte, D. Truzzolillo, F. Camerin, A. Ninarello, E. Chauveau, L. Tavagnacco, N. Gnan, L. Rovigatti, S. Sennato, E. Zaccarelli, Two-step deswelling in the volume phase transition of thermoresponsive microgels, Proc. Natl. Acad. Sci. 118 (37) (2021) e2109560118.
[54] S. Plimpton, Fast parallel algorithms for short-range molecular dynamics, J. Comput. Phys. 117 (1) (1995) 1–19. https://doi.org/10.1006/jcph.1995.1039
[55] J.B. Hubbard, J.F. Douglas, Hydrodynamic friction of arbitrarily shaped brownian particles, Phys. Rev. E 47 (5) (1993) R2983. https://doi.org/10.1103/PhysRevE.47.R2983
[56] W. Xue, S. Champ, M.B. Huglin, Observations on some copolymerisations involving N-isopropylacrylamide, Polymer 41 (20) (2000) 7575–7581. https://doi.org/10.1016/S0032-3861(00)00171-3
[57] T. Hoare, R. Pelton, Characterizing charge and crosslinker distributions in polyelectrolyte microgels, Curr. Opin. Colloid Interface Sci. 13 (6) (2008) 413–428.